NIST Special Publication 1158

Greenhouse Gas Emissions and Dispersion

1. Optimum Placement of Gas Inlets on a Building Rooftop for the Measurement of Greenhouse Gas Concentration

Kuldeep Prasad
Anthony Bova
James R. Whetstone
Elena Novakovskaia

http://dx.doi.org/10.6028/NIST.SP.1158

National Institute of Standards and Technology
U.S. Department of Commerce

NIST Special Publication 1158

Greenhouse Gas Emissions and Dispersion

1. Optimum Placement of Gas Inlets on a Building Rooftop for the Measurement of Greenhouse Gas Concentration

Kuldeep Prasad
Fire Research Division
Engineering Laboratory

Anthony Bova
Excet, Inc.

James R. Whetstone
Special Programs Office
Laboratory Programs

Elena Novakovskaia
Earth Networks, Inc.

http://dx.doi.org/10.6028/NIST.SP.1158

April 2013

U.S. Department of Commerce
Rebecca Blank, Acting Secretary

National Institute of Standards and Technology
Patrick D. Gallagher, Under Secretary of Commerce for Standards and Technology and Director

National Institute of Standards and Technology Special Publication 1158
Natl. Inst. Stand. Technol. Spec. Publ. 1158, 26 pages (April 2013)
http://dx.doi.org/10.6028/NIST.SP.1158
CODEN: NSPUE2

Greenhouse Gas Emissions and Dispersion

1. Optimum placement of gas inlets on a building rooftop for the measurement of greenhouse gas concentrations

Kuldeep Prasad, Anthony Bova, James R. Whetstone, and Elena Novakovskaia

Abstract

Inverse atmospheric dispersion models are used to provide measurement-based, or "top-down", estimates of greenhouse gas (GHG) emissions for comparison with input-based, or "bottom-up", estimates. To minimize uncertainty, inverse estimates require accurate measurements of GHG concentrations and meteorological data, and are improved when networks of sensor sites are used in concert. To closely approximate free stream mixing ratio values, it is widely-used practice to mount measurement equipment on isolated open-lattice towers to reduce the potential influences of a boundary layer formed by the supporting structure. However, this is often not possible when GHG concentrations are measured in urban environments, where open locations are unavailable or the use of such towers would be prohibitively expensive. In these environments, networks of rooftop-mounted sensors are more likely to be cost-effective and simpler to implement. Unfortunately, the flat-topped buildings that are typical of urban settings generate wind recirculation zones and turbulence that may interfere with rooftop trace gas mixing ratio measurements. In this study, large eddy simulations (LES) of wind flow over a large office building were performed to estimate the effect and potential error introduced by performing measurements on building rooftops as compared with free stream or tower-based measurements. Time dependent concentrations of carbon dioxide were computed at a number of locations and heights above the roof of a tall building and compared with the original input signal. Simulation results are used to develop guidelines for optimum placement of sensors on rooftop for accurate measurement of GHG mixing ratio that are necessary for atmospheric inversion models.

1 INTRODUCTION

Inverse methods for greenhouse gas (GHG) emission involve using atmospheric measurements to identify source location and emission flux [1]-[12]. Inversion techniques and top-down methods [2] are a means to independently verify emissions inventory data obtained from bottom-up estimates [3]. While inaccuracies in bottom-up estimates stem from input parameters [13] [14], top-down methods are subject to both error in measurements [8] and to uncertainty resulting from inverse dispersion estimates [1], [4], [5]. Depending on the spatial and temporal scales of the inverse problem, small uncertainties and loss of information in measurements may translate to large uncertainties in source estimates [6] [16]. Measurements of GHG concentrations and meteorological data used in inverse atmospheric dispersion models should therefore be as accurate and detailed as possible [9], [10].

GHG mixing ratio measurements for inversion analysis are usually obtained from sensors mounted on isolated, open-lattice towers [10] (usually cell phone and communication towers at a height of 50m to 100m above the ground) to reduce or eliminate the effect of the boundary layer formed by the structure on observations. Inversion studies [1], [4], [5] indicate that source prediction capability improves significantly in the immediate vicinity of the tower location. Installation of more measurement towers for obtaining GHG measurements and reducing the distance between measurement location and the sources is a way of reducing uncertainty. However, finding suitably isolated tower locations in an urban environment can be difficult and expensive. Since urban locations usually have tall buildings, there is a growing interest in mounting sensors on building rooftops to measure GHG concentrations, provide high resolution GHG mixing ratio data at several locations, and improve the accuracy of inversion analysis [3]. GHG measurements from building

rooftops (coupled with a footprint analysis) can also be used to design a network of observing points. Note that installation cost [11] associated with rooftop measurements is generally far less than that of installation on towers, and monetary losses can be correspondingly higher if the selected tower location ultimately proves to be unsuitable for inversion analysis.

If rooftop mounted sampling points are to be used for inversion analysis or as test locations for observing network design, then the measurements must be representative of GHG concentration in the atmospheric boundary layer. GHG measurements on top of buildings must consider the influence of the boundary layer contributed by the building itself as measurements can be contaminated by the presence of gases trapped by recirculation zones caused by the building as well as turbulence generated from nearby buildings. In this report, we estimate the error introduced by performing GHG measurements on building rooftops as compared with tower-based measurements, and provide guidance to optimize placement of sampling points on buildings. To accurately measure GHG mixing ratio in the free stream of the atmospheric boundary layer, two factors are critical,

- the resolution of the measurement instrument and
- location of the point where the gas sample is obtained.

Developments in measurement technology [18] and the commercial development and use of Cavity Ring-Down Spectrometers (CRDS) have made it possible to make CO_2 measurements resolved to approximately 50 ppb and with a temporal frequency of approximate 1 measurement per second. In spite of the high sensor resolution, measurements may not accurately reflect the GHG concentration in the boundary layer of the immediate vicinity where the sample is take because the sensors are not placed at appropriate locations or are not exposed to the environment that needs to be measured. The procedure to install sensors on a building is straight-forward and familiar for technicians who install communications antennas or other building mounted fixtures. The location of sensors on the rooftop is generally driven by practical aspects such as existing wiring, accessibility, aesthetics, as well as considerations of rooftop turbulence and recirculation zones. Figure 1 shows sensor inlets installed on the rooftops of the Earth Networks Headquarters building (Germantown, MD) [1] as well as pole mounted meteorological instruments. There has not been an extensive scientific study of ideal locations for installation of GHG sensors.

Ideally, building-mounted gas sensor inlets should be outside recirculation zones or boundary layers that might skew a measurement relative to ambient GHG mixing ratios. Although simple formulas exist to estimate dimensions of recirculation zones [19], they provide only rough guidance and do not account for the effect of the turbulent wake around a building or over the rooftop. To date, research focused on flow around buildings, and particularly rooftop recirculation, has been directed toward establishing the heights of rooftop stacks, to ensure that building effluents are injected above the re-circulation zones, and the location of intake vents around a building avoid internal recirculation of polluted air (see, e.g., [20]). In response to the growing need for meteorological data in urban areas, the World Meteorological Organization (WMO) and the U.S. Environmental Protection Agency have published guidelines [21], [22] for site selection and meteorological instrument exposure. However, densely developed sites (urban areas) make it difficult to conform to the standard WMO guidelines due to obstruction of airflow and radiation exchange by buildings and trees as well as anthropogenic activities. Oke [23] has provided further guidance

[1] Certain commercial equipment, instruments, or materials are identified in this report in order to adequately specify the materials used and the experimental procedure. Such identification does not imply recommendation of endorsement by the National Institute of Standards and Technology, nor does it imply that the materials or equipment identified are necessarily the best available for the purpose.

Figure 1: Rooftop sensor inlets for measuring greenhouse gases (centered in the photograph) and pole-mounted meteorological instruments [17]. Sensor inlets are located at approximately 3 m above the rooftop.

for choosing a location for an urban station and has considered the effect of variables such as temperature, humidity, wind speed and direction, precipitation, radiation and evaporation. McAlpine and Ruby [26] have used computational fluid dynamics (CFD) to determine the location of sensors on a power plant building for air quality modeling. Because of the effect of local topography, vegetation and built environment, it was determined that the top of the power plant building was an appropriate location. However, recent studies [24], [25] have indicated that GHG measurement through sensors located on building rooftops can be affected by local emissions of GHG, such as those due to ventilation from buildings and respiration from building occupants. This report adds to the existing literature on this subject by considering the effect of ventilation from rooftop outlets as well as respiration from building occupants.

We describe the results of a CFD study to evaluate the accuracy of GHG measurements made at various locations on the rooftop of a rectangular test building with a penthouse. Large eddy simulations (LES) were performed to estimate the effects of building-induced turbulence and recirculation zones on measurement locations at various points above the test building's rooftop. Simulation results were qualitatively compared with available data. The building was subjected to a synthetic signal in which the concentration of a GHG gas varies as a series of triangular spikes with decreasing duration. Measurements made at several rooftop and penthouse locations (and at various heights) were compared with the original signal to estimate error. Statistical measures were used to identify GHG measurement locations with minimal to no influence of building boundary layer. Spike durations that are captured accurately at these sampling locations are compared with those from freestream (tower) measurements. Simulations were performed to examine the effect of wind from different directions (including those that introduce asymmetry) and wind speed. The effect of exhaust from building vents and respiration of building occupants was considered. Based on the results of these simulations, we provide general guidelines for the placement of gas inlets or sensors on tall buildings in urban environments.

2 Problem Description and Model Formulation

Figure 2 is a schematic representation of wind flow over a flat-roofed building that results in a building boundary layer and vortical formations known as recirculation zones over the rooftop, as well as the windward and leeward sides of the building. As illustrated, the wind impinging on a building face will split below and above a stagnation point located slightly above the center of the

face. Wind below the stagnation zone forms an upwind vortex (as shown in Figure 2). Due to the edge effect at the top of the building, wind traveling over the rooftop will form a recirculation zone that, depending on the "fetch" (i.e., along wind length) of the rooftop, will cover a portion of the rooftop or, as illustrated in figure 2, may extend to the leeward side by several building widths.

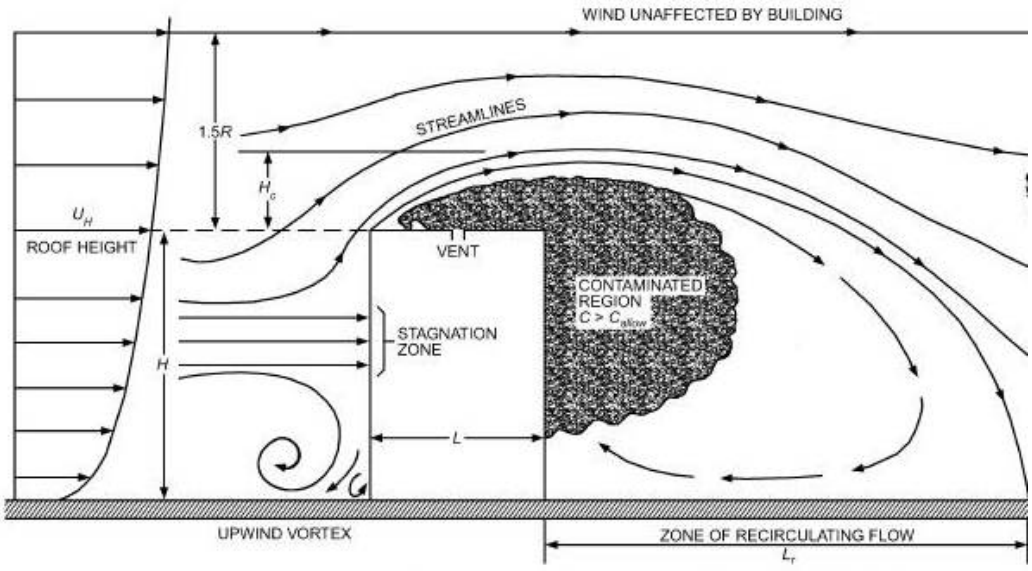

Figure 2: Illustration of flow field over a flat-roofed building. Wind with a typical atmospheric profile (U_H) from left to right results in a stagnation zone as well as recirculation zones that spans the rooftop and leeward side of the building [19].

Gases or pollutants vented on the rooftop may be trapped in such recirculation zones for an extended time, resulting in lower dilution of GHG than would otherwise occur. The same recirculation pattern that traps vented pollutants may also prevent upwind air (greenhouse gases in the atmospheric boundary layer), from entering the zone near the rooftop at mixing ratio values representative of the incoming atmosphere. As a result, mixing ratios of GHG in the free air stream may be different from that in the recirculation zone. Accordingly, it is important to place rooftop-mounted gas inlets high enough (outside the building boundary layer) so that they will be exposed to target gases carried by the free air stream. Placing tall meteorological towers on building rooftops can be expensive in terms of time and cost. Depending on their height, they may violate building codes or aesthetic sensibilities. Therefore, it is desirable to find the locations for rooftop gas inlets that guarantee exposure to air that is least affected by the building boundary layer and recirculation zones generated by wind flow over a building.

Simple formulas are available to estimate the average height and length of a recirculation zone over the rooftop of a building ([19]). However, these rough estimates do not capture the dynamics of the wind field over and around a building, especially in cases where the rooftop is not a single, flat plane, or when rooftop structures, such as large cooling units or penthouses, are present. To provide general guidelines for the placement of rooftop sensors, we performed a suite of CFD simulations to understand the flowfield around a large office building, and these calculations are described in the following sections.

3 Fire Dynamics Simulator

3.1 General Description

NIST's Fire Dynamics Simulator (FDS Version 5.5) is an open source CFD code containing a hydrodynamic solver suitable for low-speed flow (Mach <0.3), including a thermal radiation transport models. In the hydrodynamic model, a modified form of the Navier-Stokes equations are solved by a predictor-corrector scheme that is second-order accurate in time and space. Mesh cells in FDS simulations are rectilinear, and a staggered grid scheme is employed in which vector quantities, such as velocity, are assigned to cell-faces, while scalars, such as temperature, are assigned to cell centers [27]. Below we describe basic equations relevant to the GHG dispersion simulations. A detailed mathematical description of the various models in FDS is available [28].

3.2 Equation of state

In FDS, gas pressure, p, is decomposed into a "background", or static pressure, $\overline{p}(z,t)$, and a perturbation, or hydrodynamic pressure , $\tilde{p}(x,y,z,t)$. Note that z is the vertical coordinate, thus allowing for stratification of the atmosphere. The equation of state is:

$$\overline{p} = \rho T \mathcal{R} \sum_{\alpha} \frac{Z_\alpha}{W_\alpha} \equiv \frac{\rho \mathcal{R} T}{\overline{W}} \tag{1}$$

where R is the universal gas constant, T is temperature (K), ρ is density (kg/m^3), Z_α is the mixture fraction of species α, and W_α is its molecular weight (the overbar denotes a mean). Note that the equation uses the background pressure only. Atmospheric motion, and fluid motion in general, is driven by the pressure perturbation, $\tilde{p}$ [28]. For flows typical of wind and fire simulations ($\mathcal{O}(10m/s)$), the perturbation pressure is less than 1 % of the background pressure.

3.3 Large Eddy Simulations

FDS is used primarily for large eddy simulations (LES), in which fluid motion and turbulent eddies are resolved at scales greater than the mesh cell size, while the dissipative effects of turbulence at subgrid scales are modeled [27]. Although it is capable of direct numerical simulation (DNS), in which *all* spatial and temporal scales of motion are captured, this is impractical for simulations of atmospheric dispersion as the smallest atmospheric motions have dimensions of $\mathcal{O}(10^{-3}$ m), and would therefore require about 10^{15} cells in a simulation domain only 100 m on a side. The constant Smagorinsky [28] model of turbulent dissipation was used in all of the simulations below. In this model, the effects of turbulence at a subgrid scale are computed as a viscosity, μ, given by the formula:

$$\mu = \bar{\rho}(C_s\Delta)^2 \left(2\widetilde{S}_{ij}\widetilde{S}_{ij} - \frac{2}{3}(\nabla \cdot \widetilde{\mathbf{u}})^2\right)^{\frac{1}{2}} \tag{2}$$

where C_s=0.2, Δ is the characteristic dimension of a grid cell (m), $\widetilde{S}_{ij}$ is the rate of strain tensor and $\mathbf{u}$ is the velocity vector. Tildes over the variables indicate that they are resolved values, i.e., values computed from the numerical grid which, as mentioned above, is coarser than that used a DNS. Further details of the physical models and numerical methods used in FDS are available in [28].

3.4 Species Transport

In the simulations below, "air" is the implicit background gas (MW=29), while transport of the second species, CO_2 (MW=44), is modeled by solving the equation:

$$\frac{\partial}{\partial t}(\rho Z) + \quad \cdot (\rho Z \mathbf{u}) = \quad \cdot (\rho D \quad Z) \tag{3}$$

where $\mathbf{u}$ is the velocity vector (m/s), Z is the mixture fraction of CO_2, and D is mass diffusivity (m/s^2). Source terms are also included in this equation, but were omitted here as CO_2 concentration is a boundary condition and not the result of a source within the domain. The product of bulk density and diffusivity, ρD, on the right hand side is calculated from the turbulent Schmidt number, Sc, as:

$$\rho D = \frac{\mu}{Sc} \tag{4}$$

where the value of Sc is assumed to be 0.5 and the viscosity, μ, is calculated from the subgrid turbulent kinetic energy, as discussed in the section above. The diffusivity of the implicit species (air, in this case) is chosen so that the sum of all the diffusive fluxes is zero [28]. Although the formulation described above and the simulations in the following sections describe the transport of CO_2 gases, the formulation can easily be extended to other GHG species of interest such as natural gas.

4 Numerical Simulation of Wind Flow over Building Rooftops

4.1 General Configuration

We chose the NIST administrative building (Building 101) located at the NIST Gaithersburg campus as our test building for conducting the simulations. The primary reason for choosing this building is that sensor inlets can be placed on the roof of Building 101 to evaluate its effectiveness in generating accurate data for atmospheric dispersion models. In addition, the NIST Building 101 is also a large office building with a penthouse (similar to other tall urban buildings) and provides an opportunity to evaluate the performance of sensors mounted on the rooftop as well as the penthouse. The dimensions of the building (shown schematically in Figure 3) are 68 m (L) x 15 m (W) x 44 m (H). A penthouse with dimensions 28 m (L) x 10 m (W) x 6 m (H) is located near the SE corner of the rooftop. We investigated several scenarios based on prevailing wind speed, wind direction, role of building ventilation or respiration from building occupants, effects of surrounding buildings and comparison with the isolated building case as part of our computational study.

For the single isolated building case (discussed in the next section), winds were either westerly, northerly, or northwesterly (figure 3). Here we use wind directions in the conventional meteorological sense, i.e., westerly means "from the west." The westerly and northerly wind cases are considered to be worst-case scenarios because the mean wind was directly normal to either a narrow or wide face of the test building, analogous to the cases in [26]. The northwesterly wind is considered since it introduces an asymmetry in the flowfield. In the westerly and northwesterly cases, the domain (for the single isolated building case) spanned 192 m x 144 m x 150 m over the east-west (x), north-south (y) and vertical (z) axes, respectively. In the northerly case, where wind direction was perpendicular to the widest building face, the domain spanned 240 m x 240 m x 150 m, over the same respective axes, to ensure sufficient clearance between the crosswind boundaries and the building. Grid cells in the domain were 2 m cubes. The domain was split into eight separate meshes that were processed in parallel using message passing interface (mpi). The

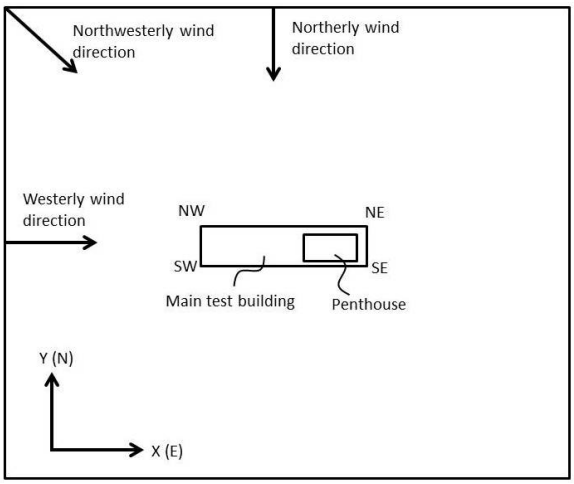

Figure 3: Plan view schematic of the simulation domain. Wind directions for each of the simulations are indicated by the arrows attached to the boundaries. Corners of the main test building are also labeled.

meshes abutted perpendicular to the direction of flow, except in the northwesterly wind case where the westerly mesh configuration was employed.

Grid convergence studies were conducted with various levels of uniform grid spacing (discussed in section 5.2.2). Based on these studies a uniform grid spacing of 2.0 m was selected. Ambient temperature in all simulations was uniform at 25° C. Ambient pressure was 101325 Pa. Wind speeds at the boundary were prescribed through a vertical profile typical of a neutrally stable atmosphere according to the power law function:

$$U(z) = U_0 \left(\frac{z}{z_0} \right)^{0.143} \tag{5}$$

where the reference height, z_0, was 10 m, a standard height above ground in meteorological studies, and U_0 was 2.5 m/s. The vertical profile roughly simulates the effect that surface drag would have on wind that has traveled over a distance much longer than the length of the domain before reaching the test building.

4.2 Introducing CO_2 in the simulations

In this study, we restrict our analysis to understanding the effect of the building on mixing ratio measurements made by sensors mounted on the roof, and comparison with tower measurements. As an example of such measurements, a time series of CO_2 concentrations from an Earth Networks meteorological tower located in Middlesex, North Carolina (35.49N, 78.90 W, Elevation 461 ft, sampling heights 50m and 95 m above ground level) is shown in figure 4 (top panel) for December 2011 [17]. Figure 4 (bottom panel) shows a portion of the data for December 13, 2011. Figure 4 (top panel) illustrates spikes of various durations both during day and night time, while the bottom panel gives a sense of the duration of the spikes. Greenhouse gas mixing ratio spike duration ranges from minutes to hours (note that the units on the horizontal axis is in days), and the data suggests that spikes with the smallest duration were of the order of approximately 60-120 s. Spike duration was consistent with data for other greenhouse gases measured at this tower, as well as those at other tower locations (GHG25 tower located in Lewisburg, Pennsylvania 40.95 N, 76.88 W). The goal of the current modeling effort is to find roof sensor locations that will give measurements of CO_2 concentration as close as possible to measurements that would be taken by instruments on an

open-lattice tower or other structure that, unlike a large building, does not have a great effect on the flow field. Another objective for this numerical study is to identify the spike durations which are not accurately resolved by roof mounted sensors, and compare the spike durations with those observed in real tower measurements.

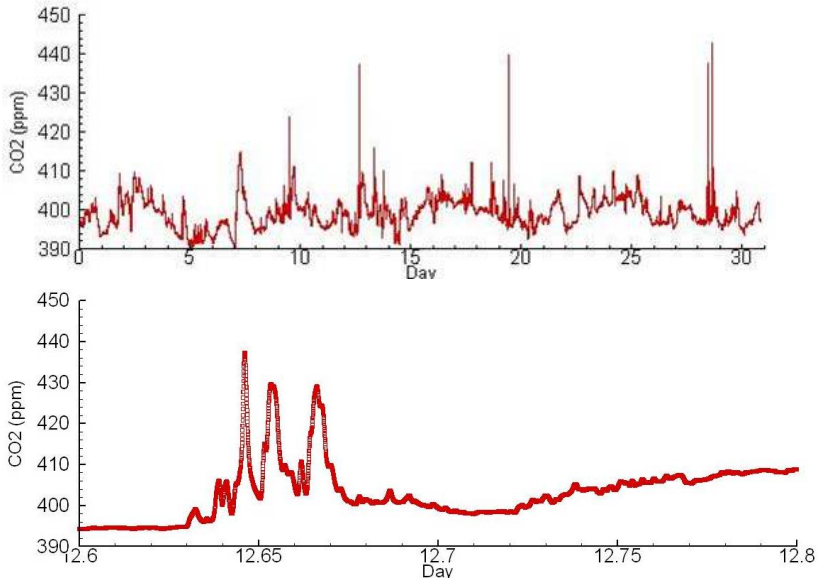

Figure 4: CO_2 concentration (ppm) plotted as a function of time for GHG 15 station located in North Carolina. Data obtained courtesy of Earth Networks. The bottom plot highlights time between 12.6 and 12.8 days.

To estimate the error associated with roof measurements, the simulated sensors mounted on a rooftop are subjected to a synthetic signal as part of a numerical study. As a proxy for the mixing ratio signal shown in Figure 4, CO_2 was injected over the entire inlet boundary as a series of spikes. The maximum amplitude of each spike was 430 ppm (i.e., 40 ppm above background of 390 ppm), but the duration of the spike events was varied as shown in Figure 5. Spike durations (600 s, 300 s, 150 s, 60 s and 30 s) chosen for this study were based on the CO_2 measurement data shown in Figure 4. Since the smallest duration of spikes observed in the tower measurement was 90 s, we chose spike durations that cover a range beginning with 90 s and extending to 600 s. The synthetic data that was imposed as a time varying boundary condition simulates the effect of upwind sources whose emissions have been uniformly mixed in the domain of interest, as well as the atmospheric transport that results in spikes at the sensor location. The spikes were introduced such that the total volumetric flow rate did not change. A tower-mounted sensor would measure the imposed spike profile without any distortion. The presence of the building boundary layer affects the sensor measurements. The difference between the two is a measure of the error, or influence of the building boundary layer on the measurements, discussed in detail in the remaining sections.

4.3 Evaluating the Influence of Building Boundary Layer on Measurements

Simulated CO_2 concentrations were recorded at points 2 m and 10 m above the rooftop at the four corners of the main test building and of the penthouse. These concentrations were compared to the original signal shown in Figure 5, which is equivalent to comparing the measurements at each location to an ideal case in which no building is present to obstruct the wind flow. Each

simulation ran for 2200 s of simulated time to allow the full sequence of spikes to pass through the domain. Concentration data were output at approximately 0.25 s intervals. To quantify the effect of the presence of the test building, the root mean squared error (RMSE) of the difference between the reference signal and concentration measurements was calculated for each of the separate wind directions. This is equivalent to finding the standard deviation of differences between the time series of the ideal, free stream, mixing rations and the building roof measurements, and can be thought of as an indicator of how measurements at a given instant differ between the two cases. RMSE were calculated separately for each CO_2 spike.

In addition, the least-squares correlation coefficient between each complete time-series of measurements and the original input signal was calculated. The coefficients indicate how closely the data at the measurement points correspond temporally to the prescribed CO_2 time series shown in figure 5. In the tables below, all coefficients were rounded to two significant digits. RMSE and correlation coefficients are considered in separate sections for each of the modeled wind directions. Data from the rooftop of the main test building and the penthouse are given in each section. To avoid clutter in the presentation, only a representative sample of windward and leeward measurements are given in the figures and tables shown in Section 5.

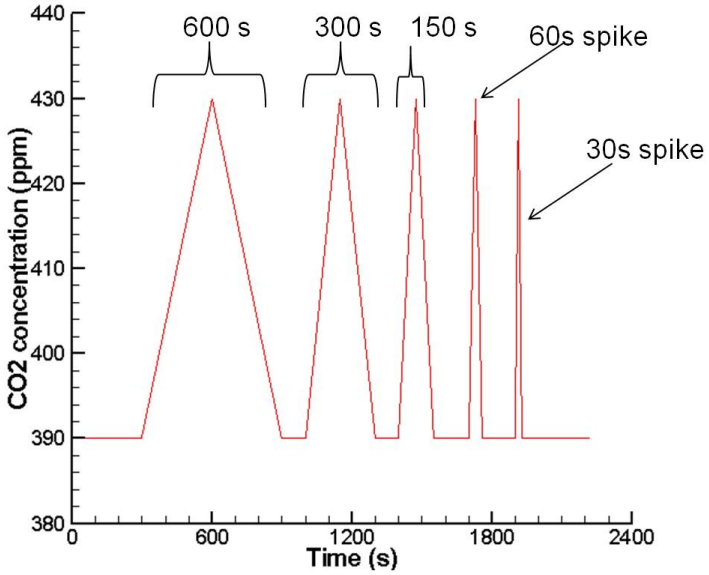

Figure 5: Prescribed CO_2 profile at inlet of domain. Spike durations are labeled.

5 Results

5.1 Westerly Wind

In the westerly wind case, the wind direction is parallel to the longest axis of the building, giving the greatest amount of rooftop fetch to affect the flow field. Figure 6 illustrates the mean velocity field obtained from an FDS simulation, averaged over 600s. Results are shown as vectors in a vertical slice through the long axis of the test building. Flow is from left to right in the image. Measurement points for concentration measurements on the building rooftop (discussed in detail in the following sections) are marked by green dots. Similarities to figure 2 are evident, including a recirculation zone on the rooftop of the main building and the penthouse, a large recirculation

zone in the lee of the building, and a flow field at the windward face of the building that is split between downward and upward directions.

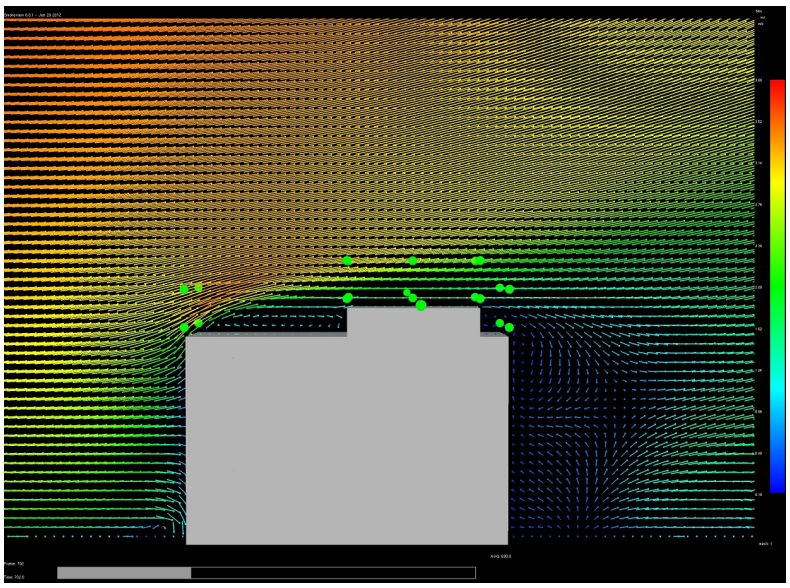

Figure 6: Average velocity vectors in a vertical slice plane through the long axis of the building. Wind flow is westerly (left to right). Vector color and length indicates velocity, with magnitudes that range from 0.1 m/s (blue) to 3.9 m/s (red). Green dots above the rooftop represent measurement locations.

CO_2 concentrations near the beginning, middle and end of the 600 s spike, are shown in the left, middle and right panels, respectively, of figure 7. Concentrations range from ambient (390 ppm, blue) to 430 ppm (red). Flow is from left to right in the figure. In each panel, CO_2 concentrations above the rooftop of the building and penthouse, as well as in the lee (right side) of the building, lag behind the concentration surrounding the building, as air in the recirculation zones mixes slowly with the ambient air. The leeward side of the main building and penthouse are exposed to turbulent flow generated over the rooftop. Note that concentrations near the windward edge of the main building are relatively unaffected by the recirculation zone and boundary layer.

Time series of CO_2 concentrations from selected sensors above the rooftop of the main test building are shown in figure 8. As mentioned, measurements from only one windward (NW) and one leeward (SE) corner of the main test building and penthouse are given as representative samples. Results are shown for a height of 2 m and 10 m above the rooftop. Due to the symmetry of the measurement points relative to the wind in this case, results at the remaining windward and leeward points are very similar to those shown. In each plot, measured values (black lines) at the selected rooftop locations are overlaid on the CO_2 reference signal (green lines). Concentrations are read on the left vertical axes of the plots. The differences between the measured and reference signal are plotted as red lines with values that are read against the right vertical axes. The red line represents the error associated with mounting the sensor inside the building boundary layer.

Windward (NW) measurements appear to closely match the prescribed signal perfectly, with very little difference between points at 2 m and 10 m above that corner of the main building rooftop (top-left and top-right panel in figure 8). The error (red line) for the windward sensors is very small for all the imposed spikes. When the sensor is located at the windward edge of the building, the height of the measurement has very little effect on the accuracy of the measurements. Results for the leeward sensors (SE) are shown in the bottom-left panel (2 m) and bottom-right panel (10 m). There is more noise in the measurements at both heights above the leeward (SE) corner, where

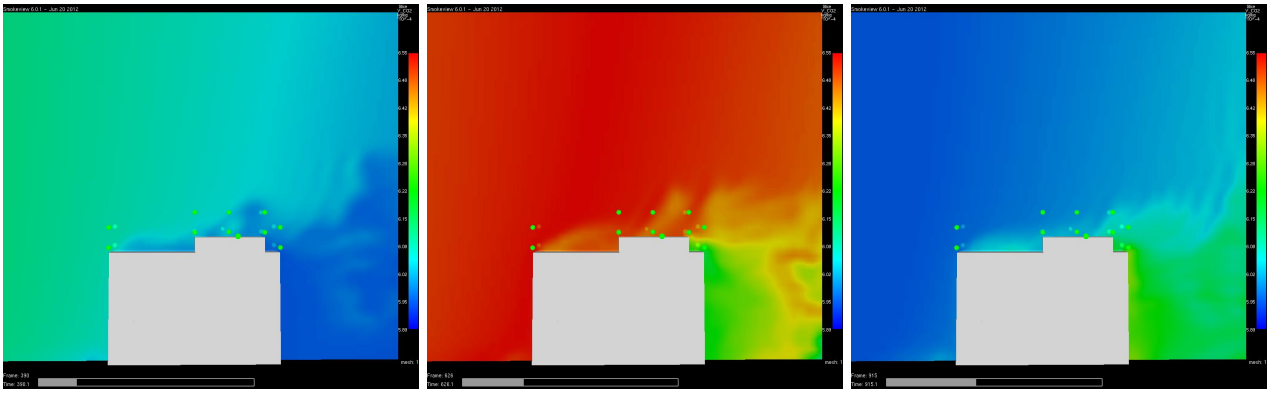

Figure 7: Vertical slices of CO_2 concentrations through the centerline parallel to the longest building axis in a westerly wind. Flow is from left to right in each panel. The penthouse rooftop is visible as a gray rectangle slightly right of center. Concentrations range from the initial value of 390 ppm (blue) to the peak value of 430 ppm (red). Green dots represent measurement locations. From left to right, the panels illustrate concentrations near the beginning, peak and end, respectively, of the 600s CO_2 spike.

differences of up to 30 ppm from the reference signal are apparent. The error curves (red lines) for these sensors indicate that the error is smaller for the duration of the 600 s spike. As the duration of the spike decreases, the adverse effects of the building boundary layer on mixing ratio measurements become much more pronounced.

Figure 9 contains time series of measurements above the penthouse in a westerly wind. The sensor mounted at 2 m above the windward (NW) corner of the penthouse shows more noise (error), while the sensor at the 10 m windward (NW) point corresponds better to the reference signal. The 10 m point is located closer to the top of the boundary layer formed over the main building and penthouse, while the 2 m point is inside the boundary layer. A rough outline of the boundary layer can be seen in the color contours shown in figure 6. Referring again to figure 6, we see that the sensors at the SE corner at both heights above the penthouse are within the boundary layer and recirculation zone formed at the top of the main building and the penthouse. Accordingly, measurements at these points appear to be equally noisy with errors of roughly the same magnitude (bottom panel of figure 9).

To better illustrate the quantitative differences between the measurements and reference signal, the RMSE for the various locations as well as for the duration of each spike are given in Table 1. Table 1 also shows the correlation coefficient for each sensor location. RMSE (ppm) at the windward (NW) corner of the main test building are very low and not significantly different at the 2 m and 10 m points. Although the RMSE values are low, they tend to increase as spike duration decreases. The correlation coefficients, rounded to two significant digits, indicate perfect agreement for these sensors. At the leeward (SE) corners of the main building, RMSE are approximately an order of magnitude larger than in the windward corner (NW). Note that the RMSE increase as the spike duration decreases, indicating poorer resolution of the original CO_2 signal over smaller time steps. Despite having higher RMSE than the windward points, the correlation coefficients are still high. The reason for this is apparent in the bottom panels of figure 8, which indicate that, despite large variability, the general patterns of rise and fall in the measurements correspond reasonably well to those in the reference signal. The RMSE and correlation coefficients of the penthouse locations (Table 1) indicate that sensors should not be mounted on the penthouse. RMSE for the penthouse

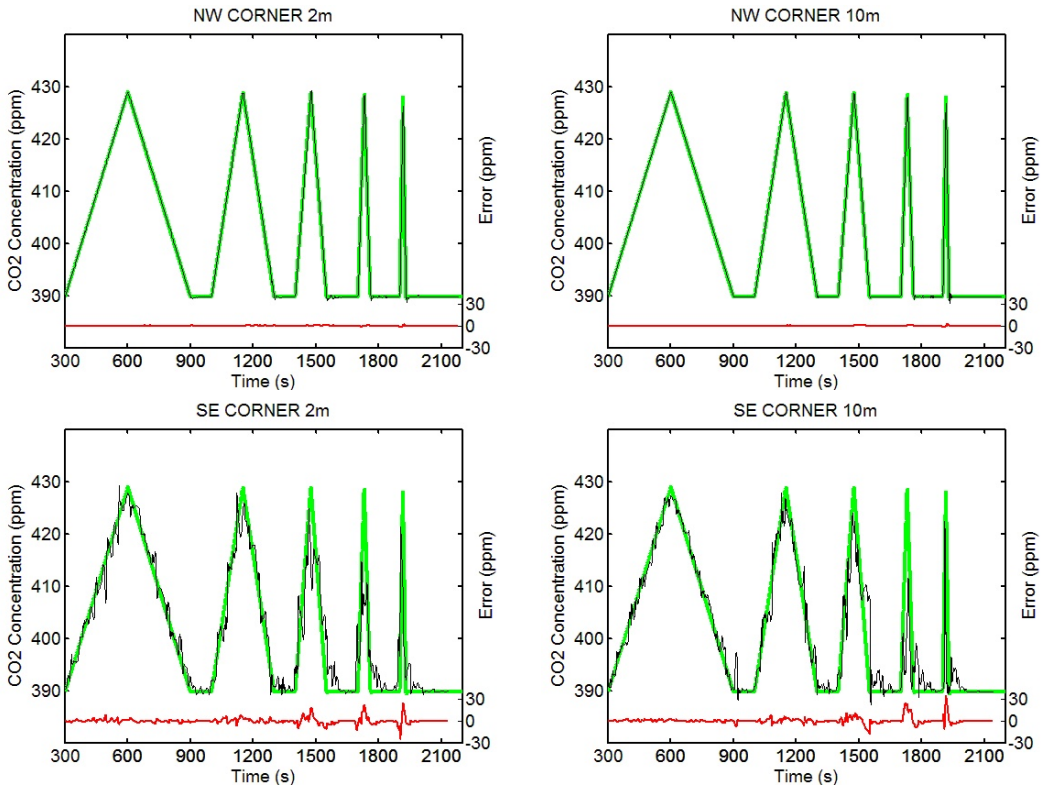

Figure 8: CO_2 concentrations at two heights above a windward (NW) and leeward (SE) corner of the main building in a westerly wind. Measured concentrations (black lines) are overlaid on the prescribed profile (green lines). Concentrations are read on the left y-axes. The difference between the two cases (error) is read against the right y-axes (red lines).

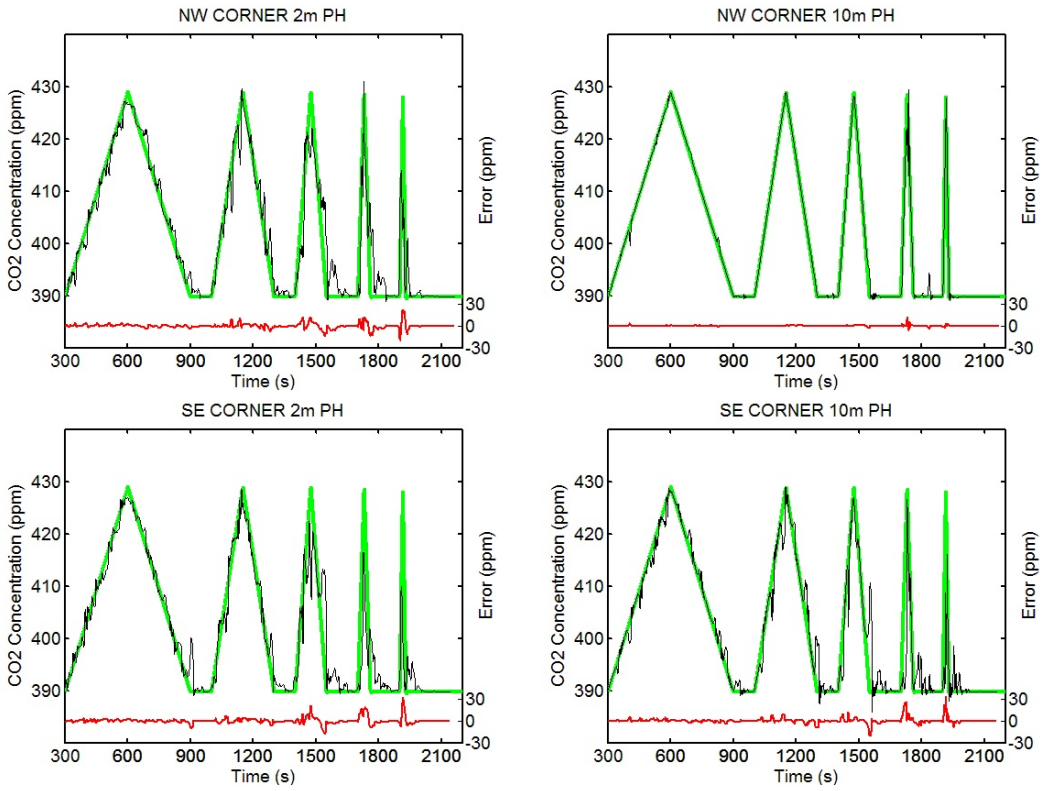

Figure 9: CO_2 concentrations at two heights above a windward (NW) and leeward (SE) corner of the penthouse (PH) in a westerly wind. Measured concentrations (black curve) are overlaid on the prescribed profile (green curve). Concentrations are read on the left y-axes. The difference between the two cases (error) is read against the right y-axes (red curve).

sensors are always higher than the corresponding sensors on the main building roof. The point 10 m above the windward corner of the penthouse gives RMSE values up to ten times lower than those at the 2 m point. Note that, despite this improvement, RMSE at 10 m above the penthouse are still higher than those of the windward points above the corners of the main building. Correlation coefficients and RMSE at the SE corner of the penthouse are similar to those above the SE corner of the main building. Unlike the windward points, the 10 m point gives RMSE that show little to no improvement over the 2 m point. Points above the leeward corner of the penthouse give higher RMSE than the windward locations.

Table 1: Westerly wind: RMSE (ppm) and correlation coefficients for various sensor locations. Times indicate spike duration.

	RMSE of CO2 spikes					
Corner Location	600 s	300 s	150 s	60 s	30 s	Correlation
NW main 2 m	0.1	0.3	0.3	0.8	1.4	1.00
NW main 10 m	0.1	0.2	0.3	0.7	1.5	1.00
SE main 2 m	1.9	2.7	6.8	7.8	15.0	0.95
SE main 10 m	1.2	2.8	6.9	8.6	12.3	0.94
NW PH 2 m	1.6	3.0	6.2	7.0	13.6	0.96
NW PH 10 m	0.4	0.3	0.8	3.2	1.8	1.00
SE PH 2 m	1.5	2.6	8.0	8.0	12.7	0.94
SE PH 10 m	1.4	3.2	4.6	8.1	9.5	0.95

5.1.1 Effects of Surrounding Buildings

In the previous section, we have considered the effect of an isolated buildings' boundary layer and recirculation zone (RZ) on rooftop mounted sensors. Results indicate that rooftop mounted sensors on the leeward sides of the building are affected by the presence of the buildings' boundary layer and RZ, while those on the windward side are relatively unaffected. The measurements made at the windward sensor will be influenced by the presence of surrounding buildings, or topography. This has not been included in the analysis. In this section, we consider the effect of turbulence generated by buildings surrounding the test building on sensors mounted on top of the test building.

In order to simulate the surrounding buildings, the domain described in section 3.1 was extended in all directions, for a total domain size of 440 m x 560 m x 150 m along the x-, y- and z-axis, respectively. The NIST administrative building is surrounded by eight large buildings. Eight blocks, each 90 m x 40 m x 10 m, were added to the domain in locations corresponding to the location of these buildings on the NIST campus (figure 10). Note that the height of the surrounding buildings (10 m) is significantly smaller than that of the test building (44-50 m). Each surrounding building was modeled as a block, and details of the surrounding buildings such as rooftop structures, were not included. Cubic grid cells in the extended portions of the domain were 10 m on an edge, while the inner domain retained its original dimensions and resolution (2 m). A westerly wind was prescribed with the same speed and profile as in the single building case described in section 3.1.

Time series of CO_2 concentrations from selected sensors above the rooftop of the main test building are shown in figure 11. These plots can be directly compared with those shown in figure 8 for the isolated building case, since the sensor locations are identical. Including the surrounding buildings in the FDS simulation introduced more noise in the measurements. The windward sensor (NW) on the main building resulted in a noisy signal due to the surrounding buildings. This was not

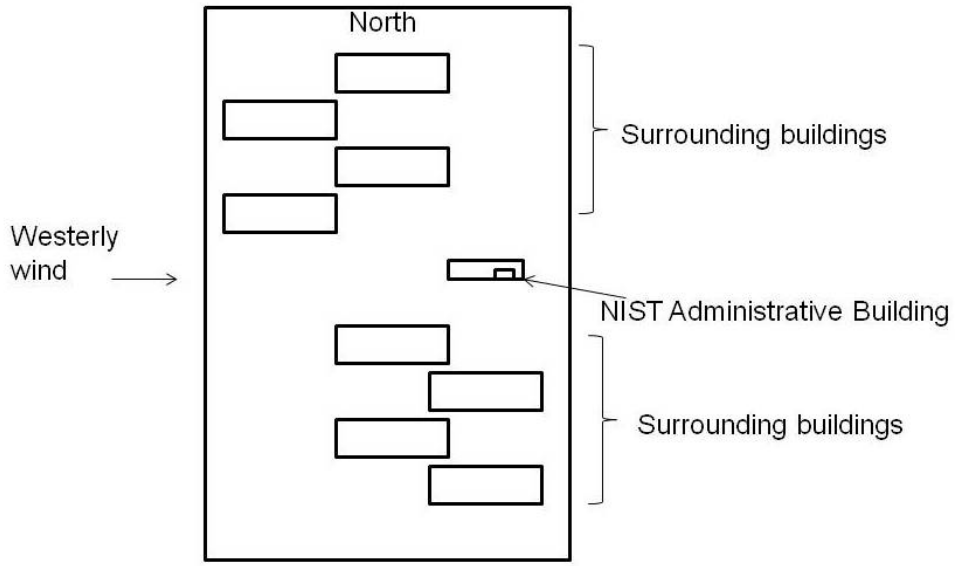

Figure 10: Extended domain showing a schematic representation of the buildings surrounding NIST Administrative Building (Building 101).

observed when the building was isolated. Measurements at the leeward side (SE) for the isolated building case and the case with surrounding buildings contain roughly the same amount of error (bottom panels of figures 11 and 8). Tables 2 shows the RMSE values and correlation coefficients for the case with surrounding buildings and this table can be compared with table 1 for the isolated building case.

As in the case above, error was evaluated by comparison with a signal (reference signal) measured by the sensors at the height of the rooftop sensors, but assuming that the building itself was not present. For the isolated building case, this signal remains more or less unaltered before reaching the windward edge of the main building. On the other hand, the presence of surrounding buildings can significantly alter the signal that is reaching the sensors mounted on top of the test building. The presence of surrounding buildings will equally affect sensors mounted on the test building or on a tower. The goal of this study is to predict the differences in measurements that would occur if building rooftop sensors were used instead of tower mounted sensors. In other words, the aim is to find whether measurements at a point above a building rooftop could give the same results as instruments at the same location if no building, or if only an open-lattice tower, was present. The surrounding buildings will have the same effect on an instrument mounted on a tower or on top of another building. While it is possible to evaluate a specific case, as above, given the myriad possibilities for arrangements and heights of surrounding buildings, it is extremely difficult to make statements about such cases in general. Therefore, our focus hereon is comparing the measurements made on a tower (assumed to correspond to the prescribed inlet signal) to those made above a building that is isolated, or is at least relatively unaffected by surrounding buildings.

5.2 Northerly Wind

In a northerly wind case, flow is normal to the building face with the greatest width, resulting in a shorter rooftop fetch than in the westerly case, but generates a large recirculation zone in the leeward side of the test building. Since wind speed and direction may change many times during the course of a day and the direction is not known apriori, these simulations help to understand

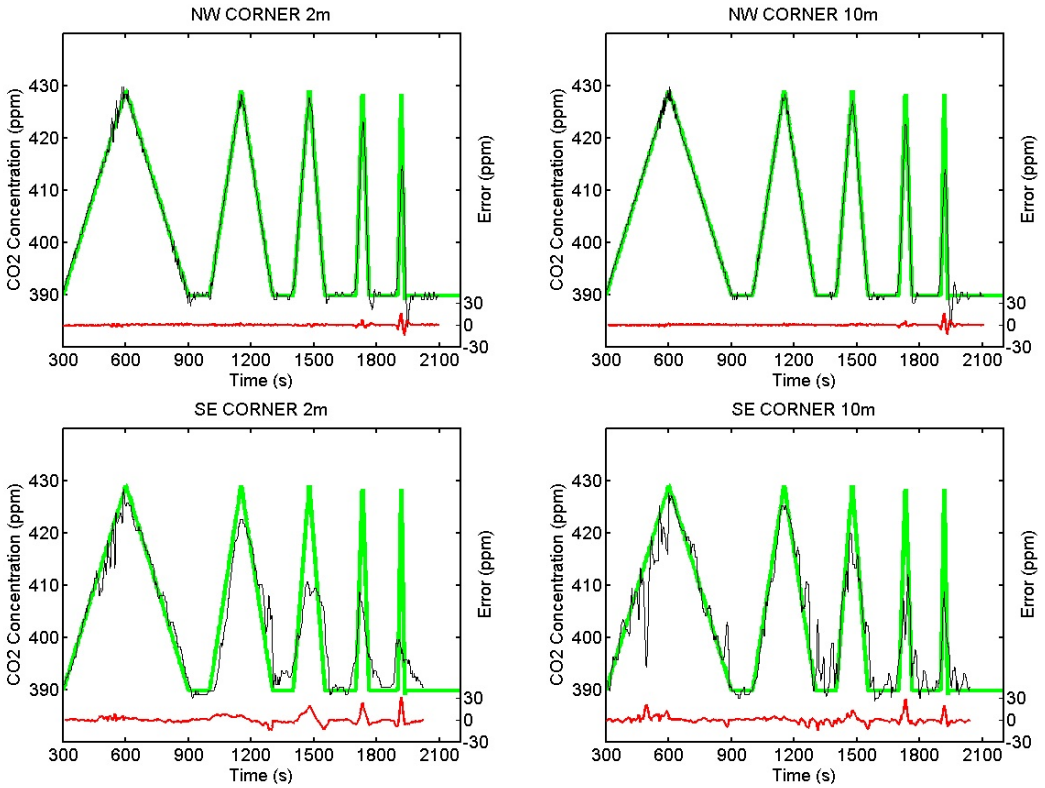

Figure 11: CO_2 concentrations in a westerly wind at two heights above a windward (NW) and leeward (SE) corner of the main building. Results include the effect of surrounding buildings. Measured concentrations (black lines) are overlaid on the prescribed profile (green lines). Concentrations are read on the left y-axes. The difference between the two cases (error) is read against the right y-axes (red lines).

Table 2: RMSE (ppm) and correlation coefficients for Westerly wind case including the effects of surrounding buildings.

	RMSE of CO2 spikes					
Corner Location	600 s	300 s	150 s	60 s	30 s	Correlation
NW main 2 m	1.0	0.6	1.0	2.4	9.4	0.99
NW main 10 m	0.6	0.5	0.9	2.0	8.9	0.99
SE main 2 m	2.1	5.7	9.0	8.8	11.3	0.92
SE main 10 m	4.3	3.4	5.8	9.7	8.7	0.94
NW PH 2 m	6.3	8.3	11.6	8.6	11.2	0.73
NW PH 10 m	4.4	6.2	9.7	6.6	9.0	0.90
SE PH 2 m	5.1	5.3	8.2	11.2	12.3	0.87
SE PH 10 m	2.5	2.8	8.4	6.0	12.9	0.91

the effect of changing wind direction on rooftop mounted sensors by comparison with the westerly wind case. Moreover, since the test building has a rectangular cross-section as seen in Figure 3 (width of the building in the westerly direction is much larger than in the northerly direction), the flowfield and turbulence levels for the northerly wind case can differ significantly from the westerly wind case.

Figure 12 illustrates the simulated mean velocity field, averaged over 600s, for the northerly wind case. As in the westerly wind case (Figure 6), measurement points are marked by green dots. The mean velocity field in figure 12 indicates a persistent recirculation zone at the lower portion of the windward face (left face), as well as a large zone of recirculation and near-zero wind speed in the leeward side (right side) of the building. The leeward (right) edges of the main building and penthouse are shielded from the impinging flow by the rooftop boundary layer and leeward recirculation zone. As in the westerly wind case, recirculation zones at the windward and leeward sides of the building form regions in which CO_2 concentration lags behind the ambient concentration, though the effect is more pronounced due to the span of the building relative to the wind direction.

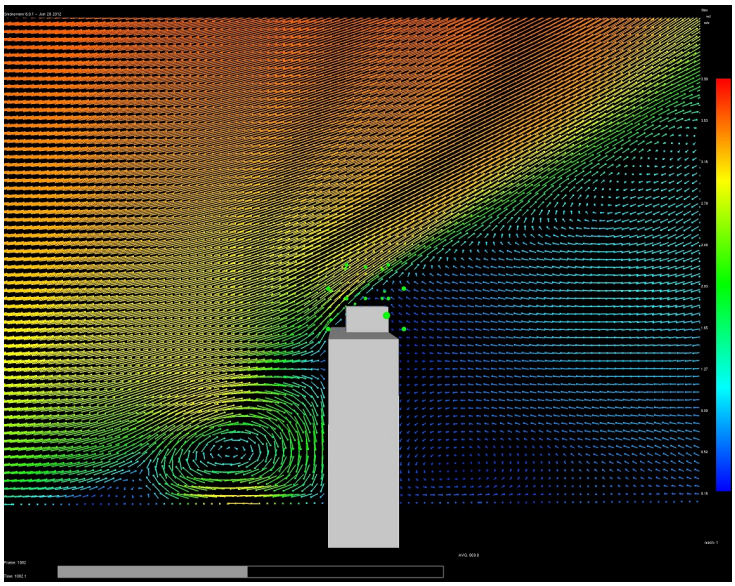

Figure 12: Vertical slice of the velocity field in a northerly (left to right) flow. Vector color and length indicates velocity, with magnitudes that range from 0 m/s (blue) to 4 m/s (red). Green dots above the rooftop represent simulated measurement locations.

Time series of CO_2 measurements above the corners of the main building for the northerly wind case are shown in figure 13. The windward (NW) points again correspond very well to the ambient concentration, with little apparent difference in accuracy between the 2 m and 10 m points. In contrast, the point 2 m above the SE corner of the main building (figure 13, lower left panel), gives noisy measurements with departures of up to about 40 ppm from the prescribed signal (i.e., from the ambient concentration). This is due to the proximity of this point to the penthouse, which is closest to that corner of the main building and produces additional turbulence and recirculation in its lee. Note that the point 10 m above the same corner (lower right panel) more closely follows the input concentration profile, as it is 4 m above the roof of the penthouse. However, its response is significantly degraded relative to the Northwest corner at the same height.

Table 3 gives the RMSE and correlation coefficients of measurements for the northerly wind case, in a format similar to the westerly wind case shown in Table 1. It is apparent that both

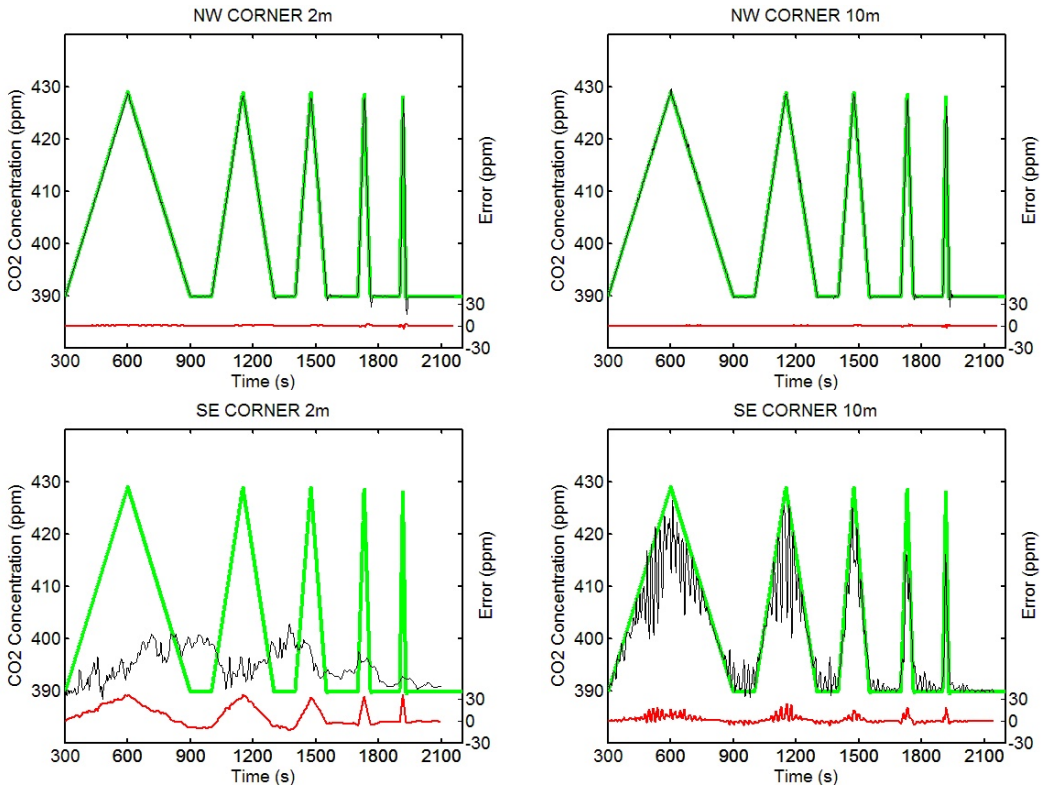

Figure 13: CO_2 concentrations at two heights above a windward (NW) and leeward (SE) corner of the main building in a northerly wind. Measured concentrations (black lines) are overlaid on the prescribed profile (green lines). Concentrations are read on the left y-axes. The difference between the two cases (error) is read against the right y-axes (red lines).

the 2 m and 10 m sensor positions at the windward (NW) location track nearly perfectly with the original signal. In contrast to the westerly wind case, the point 10 m above the leeward (SE) corner of the main building gives RMSE lower than the 2 m measurements by as much as a factor of two, indicating that the 10 m location is less heavily influenced by the rooftop RZ and wake of the nearby penthouse. Also unlike the westerly case, measurements at the 2 m leeward (SE) point in a northerly wind have relatively high RMSE for all spike durations, not just the brief spikes. As shown in figure 13 (lower left panel), the measurements at this location do not resolve the original CO_2 signal. This is reflected in the extremely low correlation coefficient for this location in table 3. RMSE values for sensors located on the penthouse are in general higher than those located on the windward side of the main building, indicating that sensor installation on top of the penthouse can lead to large measurement errors. If the height of the penthouse above the main building was significantly greater, then sensors located on top of the penthouse could be outside the wake of the main building. For such scenarios, it might make sense to install sensors on top of the penthouse.

Table 3: Northerly wind: RMSE (ppm) and Correlation coefficients for various sensor locations. Times indicate spike duration.

	RMSE of CO2 spikes					
Corner Location	600 s	300 s	150 s	60 s	30 s	Correlation
NW main 2 m	0.2	0.3	0.6	1.3	1.9	1.00
NW main 10 m	0.2	0.2	0.4	0.8	1.3	1.00
SE main 2 m	11.7	12.9	11.1	11.6	11.3	0.05
SE main 10 m	4.5	5.6	4.1	5.7	5.7	0.96
NW PH 2 m	0.5	0.5	0.6	0.9	1.7	1.00
NW PH 10 m	0.2	0.2	0.4	0.7	1.5	1.00
SE PH 2 m	10.1	10.2	9.0	10.6	13.5	0.64
SE PH 10 m	1.1	1.4	1.4	1.2	3.5	1.00

5.2.1 Effect of Mean Wind Speed

As a test for the effect of wind speed on the results, the northerly wind simulation was conducted using twice the wind speed (5 m/s) of the previous case, though with the same vertical wind speed profile. Correlation coefficients and RMSE at the corresponding locations were similar to those from the lower wind speed case, in most cases differing by not more than a few tenths of a ppm. At the higher wind speed, there were actually small improvements at both heights above the windward (NW) corner of the main building for the narrower spikes. For example, the point 2 m above the NW corner gave a RMSE of 0.8 ppm for the 60 s spike, as opposed to 1.3 ppm in a 2.5 m/s wind. The sole exceptional change occurred in the correlation coefficient at the SE corner 2 m above the main building, which increased from 0.05 to 0.26, as the wind speed increases. However, the RMSE at this point remained very similar at both wind speeds. These results suggest that the effect of wind direction is more important than the effect of wind speed at a given measurement location.

5.2.2 Grid Resolution Studies

To test the effects of mesh resolution (grid cell size) on the results, the northerly wind case was simulated using cubic grid cells of 2 m, 4 m and 6 m on a side in separate simulations. Correlations between the original CO_2 input signal and the measurements at corner locations above the main

building (see section 4.2 below) are given in table 4. The NW (windward) corners at both heights, as well as the SE corner at 2 m above the main building, show little change in correlation as cell size decreases. The same pattern was true for the SW and NE locations not shown here.

The SE (downwind) corner at 10 m shows a significant change in correlation coefficient as cell size decreases from 4 m to 2 m (table 4). However, this has less to do with the resolution of the flow field than the fact that the height of the nearby, upwind penthouse (figure 3) changes according to grid cell size. The height of the penthouse is 6 m, but its height in the simulations must conform to the grid cells in which it is located. Thus, its height is 6 m when the grid cells are 2 m or 6 m on a side, but is rounded down to 4 m when the grid cells are 4 m on a side. Because the remaining locations show convergence, or little change, of correlation coefficients as grid cell size decreases, 2 m resolution was deemed sufficient to capture the primary effects of the building on the flow field. Additional parameters, such as CPU time per simulation time step, are also given in table 4.

Table 4: Effects of mesh resolution

	Grid cell size (m)		
Parameters	2 m	4 m	6 m
NW 10 m correlation	1.000	1.000	0.999
NW 2 m correlation	1.000	1.000	0.998
SE 10 m correlation	0.367	0.784	0.817
SE 2 m correlation	0.492	0.539	0.691
CPU time / time step	0.39	0.05	0.02
Time step (s)	0.26	0.52	0.79
Number of time steps	8530	4200	2800
Total CPU time (s)	9427	1154	265

5.3 Northwesterly Wind

Simulations were performed to evaluate the effect of a Northwesterly wind on the test building and to study the effects on simulated rooftop mounted sensors. Rooftop flow due to a northwesterly wind results in a flow asymmetry around the test building relative to the wind direction. Table 5 gives the RMSE and correlation coefficients of measurements for the Northwesterly wind case, in a format similar to the westerly wind case shown in Table 1.

Low RMSE values were observed for the windward (NW) sensor and higher values for the leeward (SE) corner as in the westerly wind case. Since the sensors located on the NE corner and the SW corner also behave as windward sensors, the RMSE for these sensors was similar to that for the NW corner.

5.4 Role of Building Emissions

Exhaust vents located on building rooftops may emit CO_2 in the form of combustion products from boilers or air from a ventilation system. These gases may be trapped for extended periods in recirculation zones around buildings, as in figure 2, and could affect the readings of rooftop-mounted sensors. In addition, CO_2 resulting from human respiration may be emitted from building faces with open windows and could also be transported to rooftop locations. It is clear that leeward measurement locations, in particular, will be sensitive to these additional emissions from the building itself. However, our results suggest that a measurement location that extends horizontally

Table 5: Northwesterly wind: RMSE (ppm) and correlation coefficients for various sensor locations.

	RMSE of CO2 spikes					
Corner Location	600 s	300 s	150 s	60 s	30 s	Correlation
NW main 2 m	0.1	0.1	0.3	0.8	1.9	1.00
NW main 10 m	0.1	0.1	0.3	0.7	1.4	1.00
SE main 2 m	10.6	10.8	11.8	11.5	11.5	0.49
SE main 10 m	11.1	11.0	10.8	11.4	10.4	0.37
NW PH 2 m	1.8	1.7	2.9	2.4	8.0	0.99
NW PH 10 m	0.7	1.0	0.8	1.2	1.5	1.00
SE PH 2 m	11.6	11.8	10.9	11.3	11.8	0.13
SE PH 10 m	6.2	5.7	5.6	6.8	4.4	0.92

outward from the windward edge of a building is less likely to be affected, especially by emissions from the top of a building or building occupant respiration. Figure 14 illustrates this arrangement of the sensors. While it could be argued that emissions from a windward building face might have an effect on windward measurement locations, this seems unlikely for points that are located some distance above, and perhaps outward from, the windward edge of the rooftop, where the emissions would be swept below the measurement points.

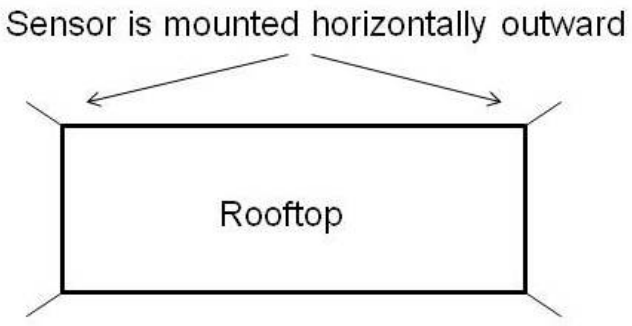

Figure 14: Schematic diagram showing the proposed location / configuration of sensors for measurement of GHG on building rooftops.

To consider the potential for use of sampling points located away from the face of a building, once can consider as an approximation, that building air ventilated through windows at a windward building face is confined to the turbulent velocity boundary layer over that face and that the flow is upward over roughly the upper half of the building. The depth, δ, of the boundary layer at the building face may be estimated from a flat plate approximation, $\delta = 0.37 x Re^{-1/5}$, where x is the distance along the direction of flow [29]. Using the half-height of the NIST's Administration Building (22 m) and a flow speed of 5 m/s (Re=7.3x10^6), the approximate depth of the layer is about 1 m when it reaches the rooftop edge. Therefore, measurement points that extend 2 m outward horizontally from the rooftop edge, are likely to be well away from the emissions confined to the boundary layer. This is likely to be a conservative estimate, as the upward flow *over* the rooftop edge is pushed leeward before it attains much height above the rooftop edge.

6 Concluding Remarks

Large eddy simulations (LES) of wind flow over a large office building were performed to estimate the influence of building's boundary layer on rooftop GHG measurements, and to compare these measurements with tower-based measurements (which closely approximates free stream measurements). Time dependent concentrations of carbon dioxide were computed at a number of locations and heights above the rooftop of the building and compared with the original input signal. Simulation results are used to develop guidelines for optimum placement of sensors on rooftop for accurate measurement of GHG mixing ratio that are necessary for atmospheric inversion models. Results are also used to identify concentration spike durations that are accurately resolved by the sensors and the spike durations are compared with those from the free stream measurements.

When concentration sensor inlets are mounted at rooftop locations, as in urban studies, simulation results indicate that they should be mounted on the windward side of the building where they are less influenced by the rooftop recirculation zone and boundary layer. This is because the building boundary layer and recirculation zone have far less effect on windward measurement points. Results also indicate that there does not seem to be an advantage in placing windward sensor inlets more than 2 m above the rooftop edge. On the leeward corner, placing sensors at 10 m above the rooftop gave smaller error as opposed to the 2 m sensor. In general, windward measurement points, whether located at 2 m or 10 m above the main test building or penthouse rooftop, are superior to the corresponding leeward measurements.

Sensors mounted on the windward side of the penthouse could be affected by the boundary layer of the main building. Therefore, installation of sensors on a penthouse should be avoided unless the height of the penthouse above the main building is large enough to avoid the main building boundary layer. Windward and leeward measurements from points above the penthouse were generally inferior to those made above the corners of the main test building.

For the particular case of NIST building 101, results suggest that an optimal configuration of CO_2 sensor inlets would be achieved by mounting them at 2 m above the four corners of the main building, thus ensuring that at least one inlet will always be windward. Measurements from the windward sensor(s) would then be used exclusively, or perhaps, weighted favorably, if the average of concentrations at all inlets is used. This approach, however, could result in large data files and would require post-processing of the sensor data before it can be used for analysis. The effect of ventilation from the building or respiration from building occupants on measurements can be further reduced by locating the sensor horizontally by a distance of 2 m beyond the windward edge of the building (Figure 14).

Generally, this strategy seems likely to be effective for a variety of building configurations. However, CFD modeling of the building targeted for use in trace gas observations should be performed to identify optimal locations, especially for complicated asymmetric building structures. In circumstances where multiple inlets cannot be used, the best strategy, based on the results above, would be to mount an inlet on the side or corner of a building closest to the prevailing wind direction. Although mounting the inlet on a pole or tower at the greatest practical height above the building, or a rooftop structure, may reduce the impact of the building's boundary layer on the measurement and reduce errors when the inlet is *not* windward, CFD simulations can aid in optimizing sensor location points. Regardless of the rooftop location(s) of GHG sensor inlets, measurements should be made on rooftops of the tallest buildings in a particular urban environment, as stated in the EPA guidelines [22]. Furthermore, the building should be chosen so that it is relatively isolated so as to avoid the effect of surrounding structures.

Simulation results indicate that it is possible to choose sensor location so as to accurately capture short duration spikes (of the order of 30 s) with acceptable levels of fidelity relative to the

free stream concentration value. It should be noted that the duration of these spikes is smaller than that observed in real tower measurement data (90 s).

6.1 Recommendations for Future Research

In future studies, the effect of building emissions should be explored through CFD simulations as well as physical experiments. A relatively simple physical experiment could involve the comparison of CO_2 concentration measurements made during weekdays versus weekends, when the number of occupants is presumably lower. In addition, measurements must be made near to or directly at exhaust vents, and at a windward building face, and these results could be checked for correlation with the target measurement points. Simulations can also be performed to estimate the effect of CO_2 exhaled by building occupants or through the building ventilation system.

Varying turbulence intensity at the inlet boundary, atmospheric stability and the presence of thermals will affect rooftop measurements and should be simulated in more detail as part of a future project, but the authors expect that these effects will be small compared to the effect of the building boundary layer.

Highly resolved simulations that can capture the detailed construction of the building exterior as well as rooftop structures can reveal the effects that these have in formation of the local boundary layer of the building. In the simulations described in this study, the buildings were modeled as a smooth-surfaced block, neglecting the detailed construction of the exterior.

7 Acknowledgements

The authors acknowledge the suggestions and support from Robert Marshall and Christopher Sloop (Earth Networks) for providing the tower data. The authors also recognize support from the entire INFLUX team, especially Prof. Ken Davis for his useful comments and suggestions.

References

[1] T. Lauvaux, M. Uliasz, C. Sarrat, F. Chevallier, P. Bousquet, C. Lac, K.J. Davis, P. Ciais, A. S. Denning, P. Rayne. Mesoscale inversion: first results from the CERES campaign with synthetic data. Atmospheric Chemistry and Physics 8:3459-3471.

[2] NRC Report, Pacala, S.W., Breidenich, C., Brewer, P.G., Fung, I.Y., Gunson, M.R., and coauthors: Verifying greenhouse gas emissions: Methods to support international climate agreements, 2010. Committee on methods for estimating greenhouse gas emissions, National Research Council, The National Academies Press, 500 Fifth Street, N.W., Washington, D.C., 20001. Available at http://www.nap.edu.

[3] E. Nisbet and R. Weiss. Top-down Versus Bottom-up. Science 328:1241-1243.

[4] Kort, E. A., J. Eluszkiewicz, B. B. Stephens, J. B. Miller, C. Gerbig, T. Nehrkorn, B. C. Daube, J. 0. Kaplan, S. Houweling, and S. C. Wofsy (2008), Emissions of CH4 and N20 over the United States and Canada based on a receptor-oriented modeling framework and COBRA-NA atmospheric observations, Geophys. Res. Lett., 35, L18808, doi:10.1029/2008GL034031.

[5] Zhao, C., A. E. Andrews, L. Bianco, J. Eluszkiewicz, A. Hirsch, C. MacDonald, T. Nehrkorn, and M. L. Fischer 2009. Atmospheric inverse estimates of methane emissions from Central California, J. Geophys. Res., 114, D16302, doi:10.1029/2008JD011671.

[6] H. W. Engl, M. Hanke, M. Liebauer. Regularization of Inverse Problems. Kluwer Academic Publishers, Dordrecht, 2000.

[7] http://climatechange.worldbank.org/content/new-report-sees-cities-central-climate-action.

[8] R. M. Duren , C. E. Miller. COMMENTARY: Measuring the carbon emissions of megacities. Nature Climate Change. Vol.2 , August 2012. `www.nature.com/natureclimatechange`.

[9] Shepson, P. B., Cambaliza, M., Davis, K. J., Gurney, K. R., Lauvaux, T. , Miles, N. L., Richardson, S., Sweeney, C. , Turnbull, J. C. , The Influx Science Team, 2010: The INFLUX Project: Indianapolis as a Case Study for the Accurate and High Resolution Determination of C02 and CH4 Emission Fluxes from an Urban Center, American Geophysical Union, Fall Meeting 2010, A13F-0279, San Francisco, CA; December 2010.

[10] Davis, K.J., Bakwin, P.S., Yi, C., Berger, B.W., Zhao, C., Teclaw, R.M., Isebrands, J.G.: The annual cycles of CO2 and H2O exchange over a northern mixed forest as observed from a very tall tower, Glob. Change Biol., 9, 12781293, 2003.

[11] http://www.earthmagazine.org/article/carbon-and-city-tracking-emissions-megacities

[12] http://www.worldbank.org/en/news/2012/06/18/rio-world-bank-launch-ground-breaking - program-low-carbon-city-development.

[13] Gurney, K.R., Law, R.M., Denning, A.S., Rayner, P.J., and coauthors: Towards robust regional estimates of CO2 sources and sinks using atmospheric transport models. Nature, 415, 626630, 2002

[14] IPCC, 2007, Climate Change 2007, The Physical Science Basis, Working Group I Contribution to the Fourth Assessment Report of the Intergovernmental Panel on Climate Change, Cambridge University Press.

[15] Prinn, R. G., R. F. Weiss, P. J. Fraser, P. G. Simmonds, D. M. Cunnold, F. N. Alyea, S. O'Doherty, P. Salameh, B. R. Miller, J. Huang, R. H. J. Wang, D. E. Hartley, C. Harth, L. P. Steele, G. Sturrock, P. M. Midgley and A. McCulloch, 2000. A history of chemically and radiatively important gases in air deduced from ALE/GAGE/AGAGE, J. Geophys. Res., 105, 17,751-17,792.

[16] I. G. Enting. Inverse Problems in Atmospheric Constituent Transport. Cambridge University Press, New York.

[17] Earth Networks, Inc. 12410 Milestone Center Dr, Suite 300, Germantown, MD 20876.

[18] Picarro Inc. Santa Clara California 95054, USA. `http://www.picarro.com`.

[19] ASHRAE. Airflow around buildings. Fundamentals Handbook, Chapter 16. 2005.

[20] B. Hajra, T. Stathopoulos, A. Bahloul (2010). Assessment of pollutant dispersion from rooftop stacks: ASHRAE, ADMS and wind tunnel simulation. Building and Environment 45:2768-2777.

[21] World Meteorological Organization 1996, Guide to Meteorological Instruments and Methods of Observation, 6th Edn., WMO-No. 8, World Meteorol. Organization, Geneva.

[22] EPA, Meteorological Monitoring Guidance for Regulatory Modeling Applications. Office of Air Quality. EPA-454/R-99-005 Environmental Protection Planning and Standards, Agency Research Triangle Park, NC 27711 February, 2000.

[23] Oke, T. R., (2004) Urban Observations, Instruments and Methods of Observation Programme, IOM Report, World Meteorol. Organiz., Geneva.

[24] Xueref-Remy, I., Quantification of CO2 emissions of Paris Megacity, Megacities Carbon Project Workshop, Caltech, Pasadena, May 2012.

[25] Wofsy, S. C., Measuring Greenhouse Gas Emissions from Urban Areas, Salt Lake City, Los Angeles, Boston, and beyond, Megacities Carbon Project Workshop, Caltech, Pasadena, May 2012.

[26] J.D. McAlpine and M. Ruby. Determining the Proper Wind Sensor Height on a Building Using CFD. Technical Proceedings of the Annual Meeting of the Pacific Northwest International Section of the Air and Waste Management Assn. 2004, Portland, OR.

[27] Mcgrattan, K. B., Baum, H. R., Rehm, R., Hamins, A., Forney, G. P., Floyd, J. E., Hostikka, S., Prasad, K., Fire Dynamics Simulator User's Guide. NISTIR 6783, U.S. Department of Commerce, National Institute of Standards and Technology, Gaithersburg, MD, 2002.

[28] J. Floyd, G. Forney, S. Hostikka, T. Korhonen, R. McDermott and K. McGrattan. Fire Dynamics Simulator Technical Reference Guide. Special Publication 1018. U.S. Department of Commerce, National Institute of Standards and Technology, Gaithersburg, MD, 2010.

[29] Incropera, F. P., DeWitt, D. P., Introduction to Heat Transfer, John Wiley and Sons, NY, 2002.

List of Figures

List of Tables